Management and design of biogas digesters: A non-calibrated heat transfer model

Vilms Pedersen, S.[a,*], Martí-Herrero, J.[c,d], Singh, A.K.[b,e], Sommer, S.G.[a,f], Hafner, S.D.[a,f]

[a] *University of Southern Denmark, Department of Chemical Engineering, Biotechnology and Environmental Technology, 5230 Odense, Denmark*
[b] *University of Southern Denmark, Centre for Energy Informatics, 5230 Odense, Denmark*
[c] *Centre Internacional de Mètodes Numérics en Enginyeria (CIMNE), Building Energy and Environment Group, Terrassa, Barcelona, Spain*
[d] *Biomass to Resources Group, Universidad Regional Amazónica Ikiam, Vía Tena-Muyuna, Km.7, Tena, Napo, Ecuador*
[e] *Present address: ESI Software Private Limited*
[f] *Present address: Aarhus University, Department of Engineering, Aarhus, Denmark.*

Abstract

A thermal balance modeling framework is developed, based on heat transfer-resistance networks. The heat transfer model accounts for effects of digester-design, location and operation, including effects of solar irradiance, external heating and ambient climate. We demonstrate extendibility of the framework by using the model in dynamic simulations of substrate temperature for digesters comprising two very different designs. Digester designs modeled include fixed-dome, buried, uninsulated and unheated household digesters in Hanoi, Vietnam, and an industrial-scale anaerobic digester located at a wastewater treatment plant in Esbjerg, Denmark. The modeled temperature profiles were evaluated against measured substrate temperatures over long periods, from 7 months and up. For the two Hanoi digesters, root-mean-square-error were 1.43 °C and 0.92 °C, with Nash-Sutcliffe model efficiency coefficients (NS-C) of 0.87 and 0.93 respectively. For the industrial digester in Esbjerg root-mean-square-error was 0.48 °C with an NS-C of 0.94. The model was not calibrated prior simulation, suggesting good predictive performance.

*Corresponding author
Email address: `svip@kbm.sdu.dk` (Vilms Pedersen, S.)

Keywords: Thermal balance model, heat transfer resistance network, anaerobic digestion, non-calibrated model, dynamic simulation

1. Introduction

Approximately 3 billion people heat their homes and cook their food by burning solid fuels over open fires, resulting in elevated air pollution levels indoors (WHO, 2016) causing more than 4.3 million premature deaths annually (WHO, 2016). In these homes, biogas produced with low-cost unheated digesters can offer a cleaner and renewable alternative to solid fuel combustion. It is estimated that around 35 million domestic digesters have been built in South-, East- and Southeast Asia (Bruun et al., 2014; Rajendran et al., 2012), and China aims at reaching 80 million household digesters by 2020 (NDRC, 2007). Popular low-cost digester designs for household biogas production in Asia are the fixed-dome and floating drum digesters, whilst plug-flow polyethylene-bag digesters are emerging in many of the Latin American countries (Garfí et al., 2016; Martí-Herrero et al., 2014).

The aim for large, heated, industrial-scale digesters is to stabilize thermal performance of the digesters and predict the impact of management decisions on thermal fluctuations in the digester. In Denmark, more than 150 biogas plants have been established across several digester types, including community digesters, sewage plant digesters, and industrial biogas plants (Bundsgaard & Kofoed-Wiuff, 2014). For both simple and advanced designs in operation, thermal balance models can be used to forecast the digester temperature based on regional climate and weather reports as well as process conditions. Thermal balance models can also be especially useful prior construction and installation of new unheated household-scale digesters, to evaluate the need for insulation or auxiliary heating to maintain the digester temperature.

Accurate prediction of temperature fluctuations in anaerobic digesters is of paramount importance, given that temperature is a key parameter as input for kinetic reaction models to estimate biogas yield. Digester temperature is known to affect biogas production, and both low temperature and temperature fluctuations can substantially reduce production rates (Peck et al., 1986; Alvarez & Lidén, 2008; Massé et al., 2003). For heated digesters, with fixed and controlled temperature, the biogas yield is easily estimated with known kinetic models, and the main issue pertains to the amount of energy required to heat the digester. However, for unheated digesters the temperature of the system is not fixed *a priori*. Reactor temperature will therefore be dynamic, depending strongly on the interaction of the system with its surroundings. Thus, a thermal balance model permits estimating the energy requirements and the temperature at which anaerobic digestion will take place, and use it as input for mass balance- and kinetic models.

Prior studies have developed heat balance models predominantly aimed at digester designs prevalent in semi-periphery and periphery countries. Axaopoulos et al. (2001) developed a 1-D thermal balance model coupled to a methanation model developed by Chen & Hashimoto (1978), used for underground solar panel heated digesters. Gebremedhin et al. (2005) developed a similar model, including the contributions of heat supplied by solar insolation and heat exchange with the ground, to manage plug-flow digesters at steady temperature. Perrigault et al. (2012) presented a 1-D thermal balance model for small buried, tubular, plug-flow PVC digesters covered by a greenhouse. The model, written in MATLAB, was developed for and evaluated against an experimental digester located on the peruvian *Altiplano*, in a cold climate known to experience significant diurnal temperature fluctuations. All major modes of heat transfer were exhaustively modeled including solar insolation, radiative heat transfers, convective heat transfers, heat exchange with the soil as well as heat transfer caused by mass flow in- and out of the reactor. Comparing slurry temperature data from the experimental digester in Cusco, Peru, to those predicted by the model gave a standard error of 0.47 °C after calibration of the model to measured slurry temperatures, over a 5 d period. A similar 1-D finite-difference model was developed for buried, unheated, fixed-dome digesters by Terradas-Ill et al. (2014).

The development of heat transfer models for anaerobic digestion systems have generally been centered around modeling a single geometry, and evaluated over short periods of time (< 1 month). The aim of this study was to develop a model that could be used as a decision-support tool for improving thermal performance of existing digesters, and to design new digesters. To achieve this aim, we have developed a new and flexible resistance network-based heat transfer model. Through a conceptual framework the heat transfer model can be applied to predict reacting material temperature for different digester geometries and configurations. Specifically, we have addressed the aim through four objectives: 1) develop a simple but accurate thermal balance model that can be applied to various digester geometries and types without prior calibration, 2) evaluate the model by comparison to experimental observations over long periods (> 7 months), 3) demonstrate flexibility by modeling very different digester designs, from unheated, uninsulated household-scale to complex industrial-scale anaerobic digestion reactors and 4) build the model as a self-contained entity, with all sub-models presented and included in the coded version of the model. This is done with a view to facilitating the use of the model as a decision-support tool, irrespective of hardware performance and access to internet.

2. Materials and Methods

2.1. Model development

The heat resistance network-based thermal balance model is aimed for simple and complex digester types, and was developed with view to: 1) minimizing the use of non-trivial input parameters, which may not be available in some regions of semi-periphery and periphery countries; 2) reducing the complexity of the model sufficiently to give near-instantaneous model solutions to the user; and 3) developing a model with good predictive performance that does not rely on model calibration. Input parameters for the model are given in Table 1. The model was developed in Mathematica®10.4.1.0 (Wolfram Research, Inc., Champaign, IL, USA). A simplified version of the code has been written in the open-source language *R*.

Table 1: Input parameters for the heat transfer resistance network-based model

Location	**Digester**	**Material flows**	**Ambient**	**Simulation Control**
Longitude	Surface area of digester walls and cover	Inlet flowrate	Air temperature	Start date
Latitude	Volume of liquid medium	Inlet temperature	Wind speed	Days of Simulation
Meters above sea level	Level of liquid medium in digester		Sky Transmissivity[a]	Time step
Time zone from GMT	Digester tank wall material			Initial conditions
	Characteristics of insulation			
	Placement			
	Auxiliary heating			

[a] Sky transmissivity (or coefficient of transmissivity) describes the atmospheric transmission of solar irradiance. On cloudy or foggy days, the transmissivity of the atmosphere decreases.

2.1.1. Model assumptions

To develop a flexible and computationally fast thermal model a number of assumptions were made. These are as follows:

1. Each element is characterized by a single temperature (substrate, air, sky). This also implies that thermal gradients in the slurry are negligible, as suggested by studies of thermal gradients in Danish storage tanks containing digested municipal organic waste, covered with floating straw (Hansen et al., 2006).
2. Soil temperature is assumed to vary by depth, considering damping of oscillations and increasing time-lags as a function of depth. The temperature at any given depth is however considered constant across the horizontal plane.
3. Soil thermal properties are considered uniform, independent of depth and time.
4. Heat transfer by evaporation from bulk liquid volume is negligible (Kishore, 1989).
5. The coefficient of transmissivity in the solar irradiance sub-model is constant over the year and based on average conditions of the regional climate.

6. Slurry volume is considered constant throughout the simulation, i.e. the feeding rate of influent feedstock equals that of the effluent digestate.
7. The substrate has the same thermal properties as water.
8. Surface-to-surface radiation inside the digester is negligible.
9. Gas in the digester head-space does not absorb heat radiated in the system.
10. Microbial heat generation is negligible under anaerobic conditions. Different pathways of methanogensis will have different enthalpies of reaction, including endothermic and exothermic contributions (Daverio et al., 2003; Fey & Conrad, 2000). Overall, the anaerobic digestion process is under many circumstances weakly exothermic, however insignificant compared to other heat transfer flows in the system, why it is frequently considered negligible in the literature of thermal balance models for anaerobic digesters (Perrigault et al., 2012; Weatherford & Zhai, 2015; Gebremedhin et al., 2005; Gebremedhin & Inglis, 2007; Terradas-Ill et al., 2014).
11. The cover is considered a radiation-shield, limiting radiative heat transfer between the digester substrate and the sky.
12. Convective heat transfer coefficients are constant.

2.1.2. Substrate energy balance and conceptual overview

In this resistance network-based model, only the temperature of the substrate is explicitly modeled. An energy balance is developed, which reduces to an ordinary differential equation (Eq. 1).

$$\begin{aligned}\rho C_p V_{sub}\frac{dT}{dt} = &\sum Q_{ADV,feeds-sub} + \sum Q_{RAD,sky-sub} + \sum Q_{IRR} \\ &+ \sum Q_{CON,air-sub} + \sum Q_{CON,gr-sub} + \sum Q_{heating}\end{aligned} \tag{1}$$

where ρ is the density of the digester substrate ($\mathrm{kg\,m^{-3}}$), C_p is the specific heat capacity of the substrate ($\mathrm{J\,kg^{-1}\,K^{-1}}$) and V_{sub} is the volume of the substrate ($\mathrm{m^3}$). dT/dt is the time-derivative of temperature, where T is temperature (K), and time t (s). Rate of heat loss (or gain), is given by Q (W), where $Q_{ADV,feeds-sub}$ is heat transfer by advection with influent substrates, $Q_{RAD,sky-sub}$ refer to heat exchange by radiative heat transfer between the sky and the substrate, and Q_{IRR} is heat gain by solar irradiance. The terms $Q_{CON,air-sub}$ and $Q_{CON,gr-sub}$ refer to heat transfer from the ambient air temperature and by heat exchange with surrounding soil, respectively (subscript CON denotes resistance lumped convection/conduction modes of heat transfer). $Q_{heating}$ is heat gain by methods of external heating, such as heat exchangers and boilers.

To ensure flexibility and fast computational execution, the model was developed as a 1-D time-dependent model. Each heat transfer rate in Eq. 1 is represented as a series of heat transfer resistances lumped into overall heat transfer coefficients. The addition of extra insulation or radiation shields can thus easily be included by modifying the thermal resistances. A schematic of the two systems used for evaluation of the model (including resistances for convective, conductive, radiative and advective heat transfers, solar irradiance and the corresponding heat transfer rates from Eq. 1) is given in Fig. 1.

2.1.3. Solar irradiance sub-model

The global solar irradiance S_{tot} ($\mathrm{W\,m^{-2}}$) at a given point in time was calculated as the sum of direct irradiation on a horizontal surface (S_b), and the diffuse irradiation on a horizontal plane from the sky (S_d), given in Eq. 2 (Campbell & Norman, 1998).

$$S_{tot}(t) = S_b(t) + S_d(t) \tag{2}$$

Reflected radiation S_r (albedo) was calculated as the product of the global solar irradiance, S_{tot}, and a surface reflectance coefficient, Γ (dimensionless) (Campbell & Norman, 1998).

$$S_r(t) = \Gamma S_{tot}(t) \tag{3}$$

According to Campbell & Norman (1998), the reflectivity coefficient Γ is 0.24 to 0.26 for grass and 0.08 to 0.18 for bare soils. The solar irradiance on tilted surfaces is given by Eq. 4 (Honsberg & Bowden, 2017).

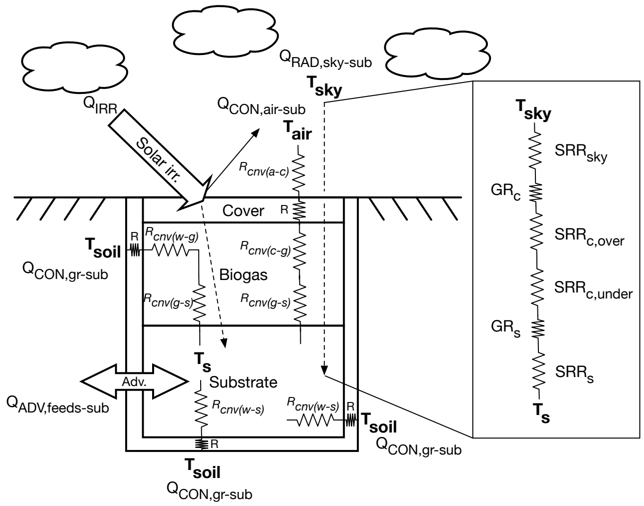

(a)

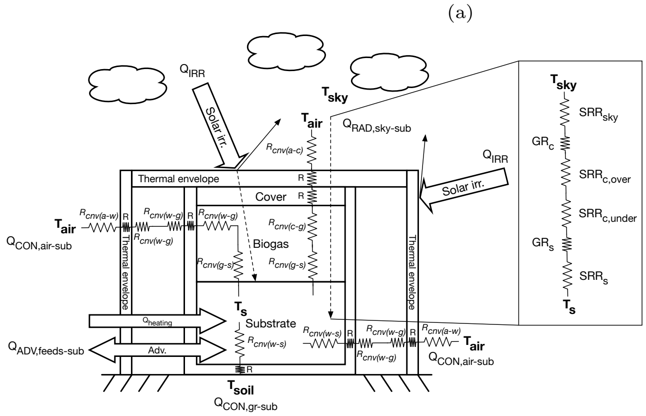

(b)

Figure 1: Setup of a resistance network-based, time-dependent, thermal balance model. $R = \Delta x/k$ denotes conductive layer resistance, where Δx (m) is the thickness of the conducting material, and k ($\mathrm{W\,m^{-1}\,K^{-1}}$) is thermal conductivity of the material. $R_{cnv\,(i-j)} = 1/h_{i-j}$ indicates convective heat transfer resistance between elements i and j, where h ($\mathrm{W\,m^{-2}\,K^{-1}}$) is the convective heat transfer coefficient. GRR ($\mathrm{m^{-2}}$) and SRR ($\mathrm{m^{-2}}$) are geometric and surface radiation resistances, respectively. Subscripts, a = air, c = cover, w = wall, g = gas, gr = ground and s and sub = substrate. Heat transfer rates Q are marked according to Eq. 1, adjacent to their corresponding resistor network, for (a) fixed-dome digesters in Hanoi, Vietnam, and (b), industrial anaerobic digester at Esbjerg wastewater treatment plant.

$$S_{tilted} = S_{incident} \frac{\sin(\alpha + \beta)}{\sin \alpha} \tag{4}$$

Where α is the sun's elevation angle, and β is the angle of the tilt of the plane to the horizontal surface. The total solar heat flux q''_{solar} ($\mathrm{W\,m^{-2}}$) is the sum of the global irradiance and albedo radiation:

$$q''_{solar}(t) = S_{tot}(t) + S_r(t) = S_b(t) + S_d(t) + S_r(t) \tag{5}$$

Heat gain by solar irradiance Q_{IRR} is calculated as the product of the solar heat flux q''_{solar}, surface area A ($\mathrm{m^2}$) of element exposed to the solar irradiance, and that element's absorptivity η (dimensionless) (Eq. 6).

$$Q_{IRR} = q''_{solar} A \eta \tag{6}$$

The heat flux by direct irradiation on a horizontal surface was calculated as the direct irradiation on a plane perpendicular to the solar beam, S_p ($\mathrm{W\,m^{-2}}$), multiplied by the sine of the sun's elevation angle θ (Gebremedhin et al., 2005; Terradas-Ill et al., 2014).

$$S_b = S_p \sin \theta \tag{7}$$

Campbell & Norman (1998) reported that S_p could be calculated as the product of the extraterrestrial flux density normal to the solar beam, and the coefficient of transmissivity raised to the power of the optical air mass number (Eq. 8).

$$S_p = S_{p0} a^m \tag{8}$$

where S_{p0} is the extraterrestrial flux density normal to the solar beam (in this model set as a constant $1360\,\mathrm{W\,m^{-2}}$ (Campbell, 1977)), a is the coefficient of transmissivity (dimensionless) and m is the optical air mass number (dimensionless). In this model, a was constant, set to reflect the average conditions of atmospheric transmissivity (Campbell, 1977).

Assuming negligibility of atmospheric refraction effects, the optical air mass number m used was that given by Campbell & Norman (1998):

$$m = \frac{\frac{P}{P_0}}{\sin\theta} \tag{9}$$

P and P_0 are the pressures at the location of the site and at sea-level respectively. P_0 is assumed equivalent to a standard atmosphere (101 325 Pa, Mohr et al. (2015)) Numerous models exists that calculates the atmospheric pressure as a function of altitude. In this model, P (Pa) was found by Eq. 10 (Wallace & Hobbs, 2006).

$$P_{Z_{alt}} = P_0 \exp\left(-Z_{alt}/8000\right) \tag{10}$$

where Z_{alt} refers to the altitude of the location in meters above sea-level (m). The sun's elevation angle θ (Eq. 7 and Eq. 9) is a function of location latitude l_t (°), the solar declination angle δ (°), and the hour angle, Ω (°) (Campbell & Norman, 1998).

$$\theta = \arcsin\left(\sin l_t \sin\delta + \cos l_t \cos\delta \cos\Omega\right) \tag{11}$$

The solar declination angle δ is given by:

$$\delta = 23.45 \times \frac{2\pi\left(doy + 284\right)}{365} \tag{12}$$

where doy denotes the day of year. The hour angle, Ω of Eq. 11, is given by $\Omega = 15\left(LST - 12\right)$ (Honsberg & Bowden, 2017), where LST is the local solar time given by Honsberg & Bowden (2017):

$$LST = LT + \frac{TC}{60} \tag{13}$$

LT refers to the local time at the location and TC is a time-correction factor as used by Honsberg & Bowden (2017) – a function of the equation of time

(EoT, in min) and the Local Standard Time Meridian (LSTM, Eq. 14 – Eq. 17). Δt_{GMT} is the difference from Greenwich Mean Time to the Local Time (h) (Honsberg & Bowden, 2017).

$$TC = 4\left(l_o - LSTM\right) + EoT \tag{14}$$

$$EoT = 9.87\sin\left(2B\right) - 7.53\cos\left(B\right) - 1.5\sin\left(B\right) \tag{15}$$

where

$$B = \frac{2\pi}{365}\left(doy - 81\right) \tag{16}$$

and

$$LSTM = 15\Delta t_{GMT} \tag{17}$$

2.1.4. Heat transfer by advection

Heat gained (or lost) by advection with influent substrate, $Q_{ADV,feed-sub}$, was calculated based on the principles of thermodynamics (Eq. 18).

$$Q_{ADV,feed-sub} = \dot{m}_{feed}C_{p,sub}\left(T_{feed} - T_{sub}\right) \tag{18}$$

where $\dot{m}_{feed}$ is the mass flow rate of influent feedstock ($\mathrm{kg\,s^{-1}}$) on a given day, $C_{p,sub}$ is the specific heat capacity of the substrate ($\mathrm{J\,kg^{-1}\,K^{-1}}$), T_{feed} is the temperature of the influent feed (K), and T_{sub} is the temperature of the substrate already in the digester (K). Influent feedstock was assumed to be of the same thermal properties as the substrate in the digester.

2.1.5. Convective and conductive heat transfer

Convective and conductive heat transfers are lumped into an overall heat transfer coefficient, U_{i-j} ($\mathrm{W\,m^{-2}\,K^{-1}}$). The heat transfer rate is calculated by Eq. 19.

$$Q_{CON,i-j} = AU_{i-j}\Delta T \tag{19}$$

where A is the area available for heat transfer between elements i and j (m^2), and ΔT is the temperature difference between the elements (K). For convective and conductive heat transfer, thermal resistances are given by Eq. 20 and Eq. 21, respectively.

$$R_{CNV} = \frac{1}{h_{i-j}} \tag{20}$$

$$R_{CND} = \frac{\Delta x}{k} \tag{21}$$

where h_{i-j} is the convective heat transfer coefficient between bulk fluid i and element j ($\mathrm{W\,m^{-2}\,K^{-1}}$), Δx is the thickness of the conducting layer (m), and k is the thermal conductivity of the layer material ($\mathrm{W\,m^{-1}\,K^{-1}}$). The overall heat transfer coefficient U is subsequently calculated by summing the heat transfer resistances according to the design of the system.

$$U = \frac{1}{\sum_{i=1}^{n}\left(R_{CNV,i}\right) + \sum_{i=1}^{n}\left(R_{CND,i}\right)} \tag{22}$$

2.1.6. Forced convective heat transfers

The magnitude of heat transfer rates governed by forced convection is dependent on the fluid velocity. Consequently, the convective heat transfer coefficient must be repeatedly updated to match the ambient conditions, in scenarios where forced convection is present. The average Nusselt number over a flat plate and for cross flow over a cylinder were reported by Cengel (2007) (Eq. 23 and 24):

$$Nu_{Cyl} = \frac{\left(\left(\frac{\mathrm{Re}}{282000}\right)^{5/8} + 1\right)^{4/5}\left(0.62\sqrt[3]{\mathrm{Pr}}\sqrt{\mathrm{Re}}\right)}{\sqrt[4]{\left(\frac{0.4}{\mathrm{Pr}}\right)^{2/3} + 1}} + 0.3 \tag{23}$$

$$Nu_{FlatPlate} = 0.037\ \mathrm{Re}^{0.8}\sqrt[3]{\mathrm{Pr}} \tag{24}$$

Where Re is the Reynolds number and Pr is the Prandtl number, both of which are dimensionless. The models herein runs using that $Pr = 0.7$, and Re given by:

$$Re = \frac{vL_c}{\nu} \tag{25}$$

In Eq. 25 v is the fluid velocity ($\mathrm{m\,s^{-1}}$), L_c is the characteristic length of the geometry defined as the roof diameter (m) and ν is the kinematic viscosity of the fluid ($\mathrm{m^2\,s}$). The forced convection coefficient is then given by:

$$h = \frac{k}{L_c} Nu \tag{26}$$

The heat transfer rate is then calculated as outlined in section 2.1.5.

2.1.7. Radiative heat transfer

Radiative heat transfer with the sky is included in the model under the assumption that the digester walls function as a radiation shield of the substrate (Incropera et al., 2013). Based on the radiation network approach, resistance to radiative heat transfer is characterized by either a *geometric* resistance (a feature of the view factor), *surface radiative* resistance (dependent on emissivity i.e. the material properties of the element), or the summation of several such resistances. The concept of these radiative resistances is analogous that of a lumped overall heat transfer coefficient containing layer conduction resistance terms $\Delta x/k$ and convective heat transfer resistance terms $1/h$. The schematic layout of radiative resistances shown in Fig. 1, between the effective sky temperature T_{sky} (K) and the substrate temperature T_{sub} (K), is given by Cengel (2007) (Eq. 27).

$$Q_{RAD,sky-s} = \frac{\sigma\left(T_{sky}^4 - T_s^4\right)}{\frac{1-\epsilon_{sky}}{A_{sky}\epsilon_{sky}} + \frac{1}{A_{sky}F_{sky,c}} + \frac{1-\epsilon_{c(top)}}{A_c\epsilon_{c(top)}} + \frac{1-\epsilon_{c(bottom)}}{A_c\epsilon_{c(bottom)}} + \frac{1}{A_cF_{c,s}} + \frac{1-\epsilon_s}{A_s\epsilon_s}} \tag{27}$$

where σ is the Stefan-Boltzmann constant ($\sigma = 5.670\,37 \times 10^{-8}$ W m^{-2} K^{-4}, Mohr et al. (2015)) ϵ_i (dimensionless) is the emissivity of the element, A_i is the surface area of element i (m^2), and $F_{i,j}$ is the view factor from i to j. Assuming that the sky is a perfect black-body of effective sky temperature T_{sky} ($\epsilon_{sky} = 1$), applying the reciprocity relation on geometric resistance $1/A_{sky}F_{sky,c}$ and noting that $F_{c,sky} = 1$, Eq. 27 reduces to Eq. 28, which is used in this model:

$$Q_{RAD,sky-s} = \frac{\sigma\left(T_{sky}^4 - T_s^4\right)}{\frac{1}{A_c} + \frac{1-\epsilon_{c(top)}}{A_c\epsilon_{c(top)}} + \frac{1-\epsilon_{c(bottom)}}{A_c\epsilon_{c(bottom)}} + \frac{1}{A_cF_{c,s}} + \frac{1-\epsilon_s}{A_s\epsilon_s}} \tag{28}$$

The view factor between digester cover and substrate surface was calculated using the view factor formula for two parallel, coaxial disks of radius r_i (m) and r_j (m) separated by distance Δx (m) (Cengel, 2007).

$$R_i = \frac{r_i}{\Delta x} \tag{29}$$

$$R_j = \frac{r_j}{\Delta x} \tag{30}$$

$$S = 1 + \frac{1 + R_j^2}{R_i^2} \tag{31}$$

$$F_{i,j} = \frac{1}{2}\left\{S - \left[S^2 - 4\left(\frac{r_j}{r_i}\right)^2\right]^{\frac{1}{2}}\right\} \tag{32}$$

An expression for the effective sky temperature, T_{sky} is derived from the study of long-wave radiation from clear skies by Swinbank (1963), and given by:

$$T_{sky} = 0.0552 \cdot T_{air}^{3/2} \tag{33}$$

2.1.8. Soil temperature profile submodel

Heat transfer in soil is much different than in air, given a more prominent thermal capacitance. Consequently, heat transfer in soils, and thus soil temperature, needs to take spatio-temporal effects on heat transfer into account, especially as a function of depth. The canonical approach is to consider the soil an infinite solid of uniform thermal properties. The thermal mass of the soil will then cause damping of thermal fluctuations and increasing time-lags, as a function of increasing depths. The soil temperature profile was calculated according to Eq. 34, which Campbell & Norman (1998) derived based on the assumption of 1-D heat transfer down through the depths of the soil — given homogeneous thermal properties of the soil over space and time — resulting in an expression for the soil temperature, $T_{gr}\left(z,t\right)$ (K), as a function of vertical depth z (m) and time t (hour).

$$T_{gr}(z,t) = \overline{T}_{sur} + \phi \exp\left(\frac{-z}{D}\right) \sin\left(\frac{2\pi}{365}\left(t - t_0\right) - \frac{z}{D} - \frac{\pi}{2}\right) \tag{34}$$

$$D = \sqrt{\frac{2 \cdot \alpha_{soil}}{\omega}} \tag{35}$$

$$\alpha_{soil} = \frac{k_{soil}}{\rho_{soil} C_{p,soil}} \tag{36}$$

$$\omega = \frac{2\pi}{365 \cdot 24 \cdot 3600} \tag{37}$$

$\overline{T}_{sur}$ is the annual average soil surface temperature (K) and ϕ is the amplitude of the sine curve describing the annual soil surface temperature (K), both found by fitting a sine curve to the input air temperature data file. Variable t_0 (h) is a phase constant, which was set to the number of hours from the beginning of the year to the coldest hour of the year. The damping depth D (m) is calculated using the thermal diffusivity (α, $\mathrm{m^2\,s^{-1}}$) of the soil and the angular frequency (ω, $\mathrm{s^{-1}}$), the duration of the annual temperature cycle).

Traditionally, the annual average soil surface temperature $\overline{T}_{sur}$ and the amplitude of the annual soil surface temperature fluctuations ϕ are found directly from the mean air temperature, and maximum- and minimum air temperatures of the input air temperature dataset. However, setting the annual amplitude by this approach may lead to fitting the sine-curve of the soil temperature-profile to the annual air temperature extremes, only valid for short periods of the year. Therefore, instead we found $\overline{T}_{sur}$, ϕ and phase t_0 by fitting a sine-curve to the input air temperature data (not model calibration). This approach leads to the average best predictions of the soil-temperature sub-model over the year, as it does not fix the soil model to capture temperature extremes.

2.1.9. External heating

Heat supplied to the substrate by external means is accounted for by the variable $Q_{heating}$ in the energy balance in Eq. 1. The rate of heat transferred directly to the substrate is given in Watts (W). For unheated digesters $Q_{heating} = 0$. If heat is supplied by recirculation of substrate through a heat-exchanger back into the digester, $Q_{heating}$ can be calculated using Eq. 18, replacing T_{feed} with the temperature of the outgoing stream of the heat-exchanger (recirculating back into the digester) and $\dot{m}_{feed}$ with the mass flow-rate of the same outgoing stream. Alternatively $Q_{heating}$ can be assigned a fixed value (in Watts), when modeling scenarios where heating is supplied continuously.

2.2. Experimental datasets

Slurry temperature predictions from our resistance network-based model were compared to observational data from two, buried, uninsulated, unmixed and unheated fixed-dome digesters located at the Thuyphuong Pig Research Centre, National Institute of Animal Science, Hanoi, Vietnam (21°04'53.6" N 105°46'07.7" E, recorded data kindly provided by Pham et al. (2014)). The research station is located 100 m above sea-level in a humid subtropical climate, with average minimum and maximum temperatures of 19.0 °C and 31.0 °C, respectively, from January 1st 2006, to January 1st 2014. Temperature data in the experimental fixed-dome digesters was recorded in 30 min intervals, from July 2012 to March 2013. Minimum and maximum air temperatures in the period were 9.0 °C and 37.0 °C, respectively.

The two biogas digesters were constructed from a composite material (fiberglass) with a total volume of $7\,\mathrm{m}^3$ and a working volume of approximately $5\,\mathrm{m}^3$. The digesters were buried to a depth of 2.6 m such that only the digester cover was exposed to the ambient atmosphere, leveled with the soil surface. Pig manure was used as feedstock, with 0.6 % to 1.16 % dry matter, feeding rate of $0.14\,\mathrm{m}^3\,\mathrm{d}^{-1}$, and hydraulic retention time (HRT) of 40 d.

On-site measurements of ambient air temperature are seldom available in the regions where this type of digester typically operates. Instead data from nearby weather stations or airports can be used. For this study air temperatures supplied as input to the model were obtained from Noi Bai International Airport, Hanoi, Vietnam (21°13'13.9" N 105°47'49.3" E), located approximately 15 km from the Thuyphuong Pig Research Centre (a difference in elevation of 88 m over the distance). Data was retrieved through Wolfram Alpha LLC (Wolfram Research, Inc., Champaign, IL, USA), at hourly resolution, covering the period from January 1st 2012 to January 1st 2014. Missing data were not interpolated, instead the nearest foregoing air temperature was used (11.7 % of the entries in the air temperature dataset from Hanoi were missing).

Digester temperature predictions from our heat resistance network-based model were also compared with measurements from an industrial-scale anaerobic digester (named *RT1A*) located at the wastewater treatment plant *Renseanlaeg Vest*, Esbjerg, Denmark (55°29'18.5" N 8°25'50.9" E). Technical drawings of the anaerobic digester as well as temperature and mass-flow sensor measurements in the period from January 1st 2016 to May 24th 2017 were kindly provided by Lisbet Adrian from DIN Forsyning A/S at 5 min-resolution, for the purpose of evaluation of this model. Measurements of air temperature and wind speed were obtained at hourly resolution from Esbjerg Airport (55°31'30.5"N 8°33'07.2"E, located approximately 8.5 km from the wastewater treatment plant, with a difference in elevation of 17 m over the distance), through Wolfram Alpha LLC (Wolfram Research, Inc., Champaign, IL, USA). For the air temperature dataset from Esbjerg Airport 2.4 % of the entries were missing, and 2.3 % were missing from the wind speed dataset. RT1A is of cylindrical geometry (15.6 m in diameter and 13.5 m tall), constructed in 40 cm concrete, and placed inside a thermal envelope 1.75 m from the outer wall of the digester. The working volume is max. 2500 m^3, with a hydraulic retention time in RT1A of about 20 d, before being moved to a different reactor.

2.2.1. Statistics and predictive performance

Predictions of slurry temperature from the model were compared to experimental data from two fixed-dome digesters in Hanoi, Vietnam, and a third industrial-scale digester at a wastewater-treatment plant in Esbjerg, Denmark. All statistical analysis were performed in version 10.4.1.0 of Mathematica®. Evaluation was done using linear regression, root-mean-square-error (RMSE), mean absolute error (MAE), and Nash-Sutcliffe Model Efficiency (NS-C) (see e.g. Dincer et al. (2015) and Nash & Sutcliffe (1970)).

3. Results and Discussion

3.1. Simulation input parameters for fixed-dome digesters in Hanoi

Input parameters for the model applied to the unmixed, unheated and uninsulated fixed-dome digesters in Hanoi, Vietnam, are presented in Table 2. The simulation was run for 500 d starting January 1st 2012, using a time-step of 15 min. The two variables for the soil sub-model, $\overline{T}_{sur}$ and ϕ were regressed and found to be 297.22 K (24.07 °C) and 6.84 K respectively, based on the input dataset as described earlier. Albedo radiation from the ground was neglected, as the digester cover was leveled with the soil's surface (Terradas-Ill et al., 2014), and therefore $S_r = 0 \Rightarrow q''_{solar} = S_b + S_d$.

Data regarding the feeding of slurry to the digester and influent slurry temperature were collected as a part of the dataset from Pham et al. (2014). On days where feeding was done, advection was included in the energy-balance of the slurry. It was assumed that the effluent stream of the digester is of equal volume and time-profile as the influent substrate, such that the slurry volume in the digester is constant over the entire time-domain. Furthermore, the coefficient of transmissivity of the solar sub-model was set to 0.79, corresponding

Table 2: Input parameters for model evaluation of the Hanoi digesters.

Location settings			
Parameter	**Value**	**Parameter**	**Value**
Longitude (°)	105.8	Meters above sea-level (m)	100
Latitude (°)	21.1	Time zone from GMT (h)	+7.0 GMT
Digester settings			
Parameter	**Value**	**Parameter**	**Value**
Height of digester (m)	2.6	Cover thickness (m)	0.005
Radius of digester (m)	0.93	Insulation thickness (m)	0 (Uninsulated)
Digester wall thickness (m)	0.005	Placement[a] (m)	-2.6
Cover area (m^2)	0.84	Slurry volume (m^3)	5.9
Thermal- and radiative properties of the elements			
Parameter	**Value**	**Parameter**	**Value**
Thermal conductivity of digester walls ($W\,m^{-1}\,K^{-1}$)	0.035	Emissivity of the cover (-)	0.75
Density of substrate ($kg\,m^{-3}$)	1000	Emissivity of the substrate (-)	0.67
Specific heat capacity of the substrate ($J\,kg^{-1}\,K^{-1}$)	4179	Absorptivity of the cover (-)	0.75
Soil thermal diffusivity ($m^2\,s^{-1}$)	8.0×10^{-7}		

[a] The depth at which the bottom of the digester is located. When the *height* of the digester equals the absolute value of *placement*, then the cover will be level with the soil surface.

to an average overcast day. Convective heat transfer coefficients between the elements were assumed to be constant. The convective heat transfer coefficients were determined by running the model including calculations of free convection coefficients (data not shown). This complicates execution and increases computation time significantly (many hours), and therefore an average convection heat transfer coefficient was calculated for heat transfer between each pair of interfaces, $h_{cov-air} = 3.55\,W\,m^{-2}\,K^{-1}$, $h_{cov-gas} = 2.15\,W\,m^{-2}\,K^{-1}$, $h_{gas-wall} = 2.70\,W\,m^{-2}\,K^{-1}$, $h_{gas-sub} = 2.20\,W\,m^{-2}\,K^{-1}$, $h_{sub-wall} = 177.25\,W\,m^{-2}\,K^{-1}$ and $h_{sub-floor} = 244.45\,W\,m^{-2}\,K^{-1}$. Lastly, the initial temperature of the slurry was set to 273.15 K, and the variable containing ambient air temperature was set to the air temperature at the time, as its initial value.

3.2. Simulation input parameters for industrial digester in Esbjerg

Simulation of the industrial anaerobic digesters at the local wastewater treatment plant in Esbjerg was run for 596 d starting October 6th 2015, using time increments of 15 min. The digester is located in a thermal envelope (Fig. 1b), made from a 0.9 mm aluminum profile, and 12.5 cm of mineral wool, with thermal conductivities of $237\,\mathrm{W\,m^{-1}\,K^{-1}}$ and $0.04\,\mathrm{W\,m^{-1}\,K^{-1}}$ respectively. Concrete used for digester walls were modeled with k =$1.80\,\mathrm{W\,m^{-1}\,K^{-1}}$. Convective heat transfer coefficients were the same as those used for modeling the fixed-dome digesters in Hanoi. $\overline{T}_{sur}$ and ϕ were regressed and found to be 284.50 K (11.35 °C) and 7.87 K respectively. The kinematic viscosity of air was set to $15.11 \times 10^{-6}\ \mathrm{m^2\,s^{-1}}$.

Table 3: Input parameters for model evaluation of the industrial digester in Esbjerg.

Location settings			
Parameter	**Value**	**Parameter**	**Value**
Longitude (°)	8.6	Meters above sea-level (m)	30
Latitude (°)	55.5	Time zone from GMT (h)	+1.0 GMT
Digester settings			
Parameter	**Value**	**Parameter**	**Value**
Height of digester (m)	13.5	Placement[a] (m)	-0.5
Radius of digester (m)	7.8	Slurry volume ($\mathrm{m^3}$)	2500
Digester wall thickness (m)	0.4		
Insulation thickness	Thermal envelope – see text		
Thermal- and radiative properties of the elements			
Parameter	**Value**	**Parameter**	**Value**
Thermal conductivity of digester walls ($\mathrm{W\,m^{-1}\,K^{-1}}$)	1.80	Emissivity of the cover (-)	0.75
Density of substrate ($\mathrm{kg\,m^{-3}}$)	1000	Emissivity of the substrate (-)	0.67
Specific heat capacity of the substrate ($\mathrm{J\,kg^{-1}\,K^{-1}}$)	4179	Absorptivity of the thermal envelope (-)	0.55
Soil thermal diffusivity ($\mathrm{m^2\,s^{-1}}$)	8.0×10^{-7}		

In this design albedo radiation from the ground was included in the heat balance of the digester walls, but not for the cover. As a consequence, the solar-submodel was split into three parts; 1) the cover, where both direct and diffuse insolation is included, thus $S_r = 0 \Rightarrow q''_{solar} = S_b + S_d$, 2) the sides (in the shadow), that does not recieve any direct sunlight, $S_b = 0 \Rightarrow q''_{solar} = S_d + S_r$, and 3) the sides of the digester facing directly towards the sun, in these cases, $q''_{solar} = S_b + S_d + S_r$. Whenever the albedo radiation was included in the calculation, the reflectivity coefficient Γ was set to 0.15, corresponding to the average reflectivity in urban areas (Campbell & Norman, 1998).

3.3. Evaluation of the resistance network-based thermal model

The two unheated digesters in Hanoi were of the same type and geometry, and substrate was fed in equal amounts to the two digesters. The temperatures predicted were compared to the measured daily mean slurry temperature in each of the two digesters, in the period from July 2012 to March 2013 (Fig. 2a). In most cases, model error is within 2.0 °C, which is an acceptable accuracy given the model does not require any calibration. For both digesters it can be seen that while the summer temperatures are generally predicted well by the model, the temperatures in the coldest month of the year, January 2013, are captured to lesser extent. In this month, predicted slurry temperature in digester 1 was 21.1 °C and the measured slurry temperature was 17.1 °C, whereas for digester 2 the predicted slurry temperature was 20.8 °C and the measured slurry temperature was 18.1 °C. Hence the model overestimated the digestion temperature by 3.0 °C and 2.7 °C in digester 1 and 2 respectively, during the cold season.

Plotting measured- versus predicted slurry temperatures in scatterplots indicates a systematic non-linear error (Fig. 2a insets) for the two Hanoi digesters. Despite this observation, a linear regression of the data yields a high coefficient of determination: $R^2 = 0.940$ and $R^2 = 0.947$ for *Hanoi 1* and *Hanoi 2* respectively (Table 4). This is close to the evaluated performance of the model developed by Terradas-Ill et al. (2014) where $R^2 = 0.96$. However, in their study only a subset of the data available was used for the evaluation, and model prediction compared to observational data in the period from end December 2012 to end January 2013 was not a part of the model evaluation. This could be sufficient to explain the marginally lower R^2-value of the model developed here, given that the two models are evaluated on the same experimental dataset. The linear regression analysis also indicates that for neither digester does the 95 % confidence interval of the parameter estimate of the slope suggest a 1:1 correlation between the predicted and measured slurry temperatures (Table 4). The non-linearity of the residual error between predicted and measured slurry temperatures is also seen in the time-series plots of the simulation results in Fig.

2a. The predicted slurry temperatures follow a clear sinusoidal pattern, about which the measured slurry temperatures vary.

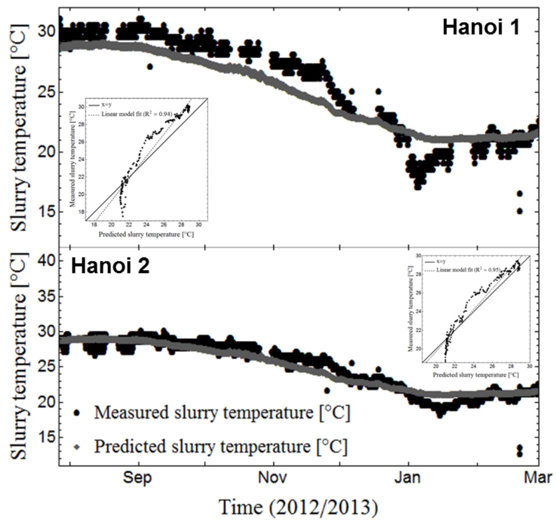

(a)

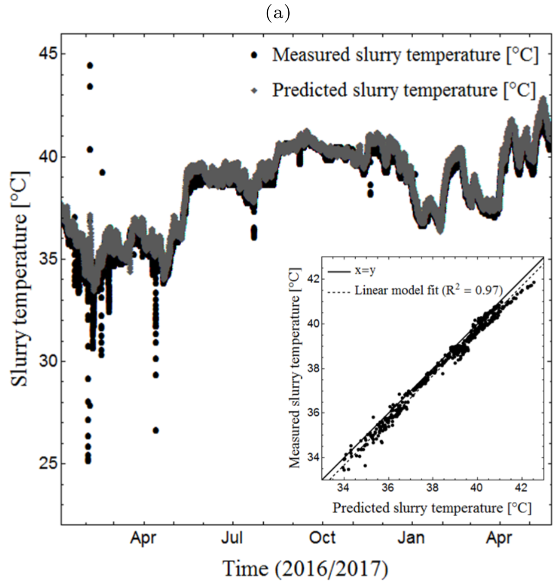

(b)

Figure 2: Predicted and measured slurry temperatures for **(a)** Hanoi 1 and Hanoi 2, **(b)** Esbjerg 1. Insets are the corresponding scatter plots of predicted- versus measured slurry temperatures. Plots have been cropped to the densest region of datapoints.

Table 4: Linear regression analysis of model evaluation scatterplots

Digester No.	Parameter	Parameter Estimate	Standard error	Confidence Interval		R^2
				Lower 95%	Upper 95%	
Hanoi 1	Slope	1.268	0.023	1.222	1.314	0.940
	Intercept	-6.006	0.584	-7.158	-4.855	
Hanoi 2	Slope	1.123	0.019	1.087	1.160	0.947
	Intercept	-2.722	0.457	-3.622	-1.822	
Esbjerg 1	Slope	1.006	0.008	0.990	1.023	0.966
	Intercept	-0.536	0.325	-1.174	0.103	

An explanation for the systematic non-linear residual error observed in the insets of Fig. 2a could be that the majority of surface area available for heat transfer ($17.9\,\mathrm{m}^2$, approximately 95.5 % of the total surface area available for heat exchange with the surroundings) is located below ground. As the soil temperature profile is essentially governed by a sinusoid function, the non-linear error could be caused by systematic over- or underestimation of the soil temperature by the sine-curve. This is further supported by a strong linear relationship between predicted slurry temperatures and predicted soil temperatures ($R^2 = 0.996$, slope $= 0.919$, 95 %-confidence interval $= \{0.917, 0.921\}$, graph not shown). A similar observation was made by Terradas-Ill et al. (2014), who suggested that substrate temperatures in buried, unheated and uninsulated digesters, can be predicted based on the measured (or predicted) soil temperature. Overall model accuracy for buried digesters hence becomes dependent on the accuracy of the soil-submodel. In this model, amplitude of soil surface temperature fluctuations were calculated by parameter estimates of the least-squares fit of a sine-function to the ambient air data. Consequently, temperatures at the extremes of the annual air temperature amplitude are likely not to be captured by the model (as indicated by Fig. 2a). Alternatively the two input parameters, ϕ and $\overline{T}_{sur}$, could have been calculated directly from the air temperature dataset as discussed earlier, however, this approach would lead to good fits near the annual temperature extremes but not during the rest of the year (results not shown). Therefore the former approach was used in this study.

For the industrial-scale digester at Esbjerg wastewater treatment plant (*Esbjerg 1*), air temperatures were obtained from Esbjerg Airport and input parameters are given in Table 3. As depicted in Fig. 1b, the setup and configuration was more complex than for the Hanoi digesters, now including a thermal envelope, additional external heating as well as albedo radiation and forced convection from winds. The time series of predicted and measured slurry temperatures are presented in Fig. 2b, where the inset is the associated scatter plot demonstrating a clear linear correlation. Predictions of slurry temperature in the digester were generally in good agreement with measured slurry temperatures, except for few observations in February and March 2016 that may have been caused by inaccurate instrument readings. Unlike the Hanoi digesters, a linear regression analysis of predicted and measured slurry temperatures in Fig. 2b (inset), suggests a direct 1:1 correlation between predicted- and measured slurry temperatures, with $R^2 = 0.966$. Predictive performance was better than for the Hanoi digesters, with a Nash-Sutcliffe Model Efficiency coefficient of NS-C = 0.94. Despite the increased complexity of the system, the proposed model performs well.

The root-mean-square-error of the resistance-network heat transfer model were for all three digesters modeled, within 2.0 °C (Table 5). The mean bias error is negative for evaluations of *Hanoi 1* and *Hanoi 2*, suggesting that the model, on average, under-predicts measured slurry temperatures by 0.018 °C and 0.009 °C respectively. Model predictions for *Esbjerg 1* on average slightly over-predicts slurry temperature (MBE = 0.008 °C). Thus, the model does not appear to induce large, systematic biases on model predictions, for the evaluated digester types. The Nash-Sutcliffe Model Efficiency Coefficient, used to assess model predictive performance, were 0.87, 0.93 and 0.94 for *Hanoi 1*, *Hanoi 2* and *Esbjerg 1* respectively, suggesting that the model is by far a better predictor than the mean slurry temperature (1 = perfect match). All evaluations were perfomed including outliers, and the model may thus perform better than described here.

A direct comparison between this heat transfer resistance-network model

Table 5: Evaluation of the resistance-network based thermal model and predictive performance

Digester No.	Mean absolute error [°C]	Mean bias error [$\times 10^{-3}$ °C]	RMSE [°C]	NS-C [−]
Hanoi 1	1.25	-1.81	1.43	0.87
Hanoi 2	0.77	-0.85	0.92	0.93
Esbjerg 1	0.32	0.81	0.48	0.94

and other thermal balance models previously made available in the literature (Perrigault et al. (2012); Terradas-Ill et al. (2014); Weatherford (2010)), is difficult. This is primarily owing to differences in the accuracy- and predictive performance evaluation methods, but also differences in the purpose of the models. Models for specific digester designs and climate conditions can be calibrated more precisely to obtain better results – but should be avoided for models whose purpose is flexibility.

3.4. Analysis of heat transfers

The development of a time-resolved resistance-network thermal heat balance model allows detailed analysis of heat transfer rates for each of the thermal resistances present in the model. We earlier hypothesized that for buried, uninsulated and unheated digesters, heat transfer between the digesters and surrounding soil would be the dominant heat transfer interface, given the strong correlation between predicted slurry temperatures and the temperature of the surrounding soil. Similarly, for the industrial-scale digester in Esbjerg we would hypothesize that process conditions in the reactor dwarfs other heat flows in the system. To test these hypotheses, we separately extracted all heat transfer rates from the respective systems, over the same duration as used for model evaluation. For the Hanoi digesters this was in the period from July 2012 to March 2013, and for the Esbjerg digester, from January 2016 to May 2017. We then grouped each heat transfer rate time-series into four categories, heat loss/gain from:

1. Advection, such as with influent substrate.
2. External heating, for instance by heat exchange with other flows in the system.
3. Conductive, convective and radiative heat transfers, at digester walls exposed to the ambient or through the soil.
4. Solar irradiance on digester surfaces exposed to the ambient.

To determine whether a given category of heat flow is a net source- or sink, we calculated the total energy transferred by integrating each of the heat transfer rate time-series over the entire duration of the evaluation period. We followed the convention that energy sinks in the system are negative valued, while sources are positive valued. While some categories can solely be net energy contributors to the energy balance, such as solar irradiance, other categories such as conductive, convective and radiative energy transfers can be both sources and sinks depending on the ambient conditions. Hence, over a given evaluation period, these categories can appear as net-zero energy contributors. To reveal dominant heat transfer interfaces we therefore also calculated the absolute energy transferred for each of the categories across digester-types, over the same evaluation period as previously described.

The biggest net energy source for *Hanoi 1* and *Hanoi 2* was solar irradiance (Fig. 3), contributing 1.82 GJ over the evaluation period. In the same period, the greatest net energy sink was conductive, convective and radiative heat transfer modes, with -2.02 GJ, which also covers heat exchange with the surrounding soil. Influent substrate was generally a net energy source over the evaluation period by 0.05 GJ, however not a significant contributor compared to other heat steams. Because the digesters were unheated, heat gain from external heating was 0. The absolute energy transfer over the evaluation period for *Hanoi 1* and *Hanoi 2* reveals that conductive, convective and radiative transfers are indeed the dominant heat transfer interface with 2.25 GJ over the evaluation period, of which 78.4 % is conductive energy exchange with the soil. Together with solar irradiance, they make up 94.6 % of the total energy budget for these fixed-dome, buried, uninsulated, unmixed and unheated digesters in the Vietnamese highlands. We thus conclude that the digester slurry temperature will be correlated with the temperature of the surrounding soil driving the heat exchange between the digester and the soil, dwarfing all other heat flows except for solar irradiance.

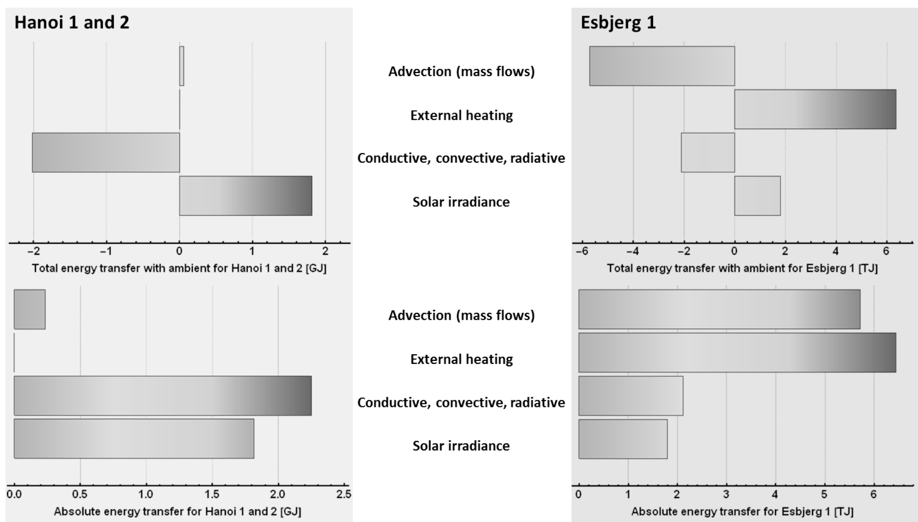

Figure 3: Total and absolute total energy budget for the Hanoi digesters (left) and the Esbjerg digester (right). Heat transfers rates were extracted for each of the elements in the thermal resistance-network, categorized into four groups, and analyzed over the same period of time as for the evaluation of the model.

The net energy budget for *Esbjerg 1* (Fig. 3) reveals that advection with influent substrate is a major energy sink in the system ($-5.72\,\mathrm{TJ}$) over the evaluation period. The net energy loss from advection is approximately of the same magnitude as that energy provided by external heating ($6.35\,\mathrm{TJ}$). Solar irradiance is unsurprisingly a net source of energy over the evaluation period with $1.76\,\mathrm{TJ}$, while conductive, convective and radiative heat transfers are combined net energy sinks of $-2.11\,\mathrm{TJ}$. As opposed to the Hanoi digesters, the absolute energy budget of *Esbjerg 1* is dominated by advection with influent substrate and external heating, totaling $12.16\,\mathrm{TJ}$ over the evaluation period, corresponding to $75.7\,\%$ of the energy budget for the industrial scale digester. Thus, not only heating of the industrial-scale digester plays a significant role on the total absolute energy budget, but also advection of influent substrate. Alternatively the effluent flow from the digester can be thought of as a major energy sink, underpinning the role of heat exchangers for an optimized energy budget. This is perhaps unsurprising, regardless, the resistance network-based thermal balance model is capable of providing a quantitative estimate of the significance of effluent mass flow as a sink.

4. Conclusions

We have developed a time-resolved 1-D resistance-network thermal balance model. The model was evaluated against two uninsulated, unmixed and unheated biogas digesters in Vietnam and an industrial-scale digester at a wastewater treatment plant in Denmark. The root-mean-square-error were 1.43 °C and 0.92 °C for the Hanoi digesters. Predictive performance was evaluated using Nash-Sutcliffe model efficiency coefficient (NS-C), and were 0.87 and 0.93 respectively. For the industrial-scale digester in Esbjerg, operation data was available for sixteen months, allowing for long-term evaluation of the model. Here the root-mean-square-error was 0.48 °C, and the predictive performance was NS-C=0.94. It is worth noting that evaluation was carried out without prior calibration of the model, indicating high predictive performance.

Acknowledgements

We would like to acknowledge and thank Knud Villy Christensen, Christian Veje and Peter Brilner Lund for numerous discussions and helpful comments on the mathematics and physics of heat transport. We would also like to thank Lisbet Adrian from DIN Forsyning A/S, for delivering operation data on Anaerobic Digester RT1A at Renseanlaeg Vest. We would also like to thank Pham et al. (2014) for kind donation of operation data from the Hanoi digesters. The authors declare no conflict of interest.

Funding

This research did not receive any specific grant from funding agencies in the public, commercial, or not-for-profit sectors.

References

[1] Alvarez, R., & Lidén, G. (2008). The effect of temperature variation on biomethanation at high altitude. *Bioresour. Technol.*, *99*, 7278–7284. doi:10.1016/j.biortech.2007.12.055.

[2] Axaopoulos, P., Panagakis, P., Tsavdaris, A., & Georgakakis, D. (2001). Simulation and experimental performance of a solar-heated anaerobic digester. *Sol. Energy*, *70*, 155–164. doi:10.1016/S0038-092X(00)00130-4.

[3] Bruun, S., Jensen, L. S., Khanh Vu, V. T., & Sommer, S. (2014). Small-scale household biogas digesters: An option for global warming mitigation or a potential climate bomb? *Renew. Sustain. Energy Rev.*, *33*, 736–741. doi:10.1016/j.rser.2014.02.033.

[4] Bundsgaard, S. S., & Kofoed-Wiuff, A. (2014). *Experiences with biogas in Denmark*. Department of Management Engineering, Technical University of Denmark.

[5] Campbell, G. S. (1977). *An Introduction to Environmental Biophysics*. Heidelberg Science Library (1st ed.). New York, NY: Springer New York. doi:10.1007/978-1-4684-9917-9.

[6] Campbell, G. S., & Norman, J. M. (1998). *An Introduction to Environmental Biophysics*. (2nd ed.). New York, NY: Springer New York. doi:10.1007/978-1-4612-1626-1.

[7] Cengel, Y. A. (2007). *Heat and Mass Transfer: A Practical Approach*. (3rd ed.). Boston: McGraw-Hill.

[8] Chen, Y. R., & Hashimoto, A. G. (1978). Kinetics of methane fermentation. In *Proc. Symp. Biotechnol. Energy Prod. Conserv.*. Gatlinburg. URL: http://www.osti.gov/scitech/servlets/purl/6534841.

[9] Daverio, E., Spanjers, H., Bassani, C., Ligthart, J., & Nieman, H. (2003). Calorimetric investigation of anaerobic digestion:Biomass adaptation and temperature effect. *Biotechnol. Bioeng.*, *82*, 499–505. doi:10.1002/bit.10595.

[10] Dincer, I., Colpan, C. O., Kizilkan, O., & Ezan, M. A. (2015). Progress in Clean Energy, Volume 2: Novel Systems and Applications. doi:10.1007/978-3-319-17031-2.

[11] Fey, A., & Conrad, R. (2000). Effect of Temperature on Carbon and Electron Flow and on the Archaeal Community in Methanogenic Rice Field Soil. *Appl. Environ. Microbiol.*, *66*, 4790–4797. doi:10.1128/AEM.66.11.4790-4797.2000.

[12] Garfí, M., Martí-Herrero, J., Garwood, A., & Ferrer, I. (2016). Household anaerobic digesters for biogas production in Latin America: A review. *Renew. Sustain. Energy Rev.*, *60*, 599–614. doi:10.1016/j.rser.2016.01.071.

[13] Gebremedhin, K. G., & Inglis, S. F. (2007). Validation of a Biogas Production Model and Determination of Thermal Energy from Plug-Flow Anaerobic Digesters. *Trans. ASABE*, *50*, 975–979. doi:10.13031/2013.23137.

[14] Gebremedhin, K. G., Wu, B., Gooch, C., Wright, P., & Inglis, S. (2005). Heat transfer model for plug-flow anaerobic digesters. *Trans. ASAE*, *48*, 777–785.

[15] Hansen, T. L., Sommer, S. G., & Christensen, T. H. (2006). Methane Production during Storage of Anaerobically Digested Municipal Organic Waste. *J. Environ. Qual.*, *35*, 830–836. doi:10.2134/jeq2005.0239.

[16] Honsberg, C., & Bowden, S. (2017). The Sun's Position. URL: http://www.pveducation.org/pvcdrom/2-properties-sunlight/suns-position.

[17] Incropera, F. P., Dewitt, D. P., Bergman, T. L., & Lavine, A. S. (2013). *Fundamentals of heat and mass transfer*. (7th ed.). Hoboken, NJ: John Wiley & Sons, Inc.

[18] Kishore, V. (1989). A heat-transfer analysis of fixed-dome biogas plants. *Biol. Wastes*, *30*, 199–215. doi:10.1016/0269-7483(89)90121-3.

[19] Martí-Herrero, J., Alvarez, R., Rojas, M., Aliaga, L., Céspedes, R., & Carbonell, J. (2014). Improvement through low cost biofilm carrier in anaerobic tubular digestion in cold climate regions. *Bioresour. Technol.*, *167*, 87–93. doi:10.1016/j.biortech.2014.05.115.

[20] Massé, D. I., Masse, L., & Croteau, F. (2003). The effect of temperature fluctuations on psychrophilic anaerobic sequencing batch reactors treating swine manure. *Bioresour. Technol.*, *89*, 57–62. doi:10.1016/S0960-8524(03)00009-9.

[21] Mohr, P. J., Newell, D. B., & Taylor, B. N. (2015). CODATA Recommended Values of the Fundamental Physical Constants: 2014. doi:10.5281/ZENODO.22826.

[22] Nash, J. E., & Sutcliffe, J. V. (1970). River flow forecasting through conceptual models part I — A discussion of principles. *J. Hydrol.*, *10*, 282–290. doi:https://doi.org/10.1016/0022-1694(70)90255-6.

[23] NDRC (2007). Medium and Long-Term Development Plan for Renewable Energy in China.

[24] Peck, M. W., Skilton, J. M., Hawkes, F. R., & Hawkes, D. L. (1986). Effects of temperature shock treatments on the stability of anaerobic digesters operated on separated cattle slurry. *Water Res.*, *20*, 453–462. doi:10.1016/0043-1354(86)90193-4.

[25] Perrigault, T., Weatherford, V., Martí-Herrero, J., & Poggio, D. (2012). Towards thermal design optimization of tubular digesters in cold climates: A heat transfer model. *Bioresour. Technol.*, *124*, 259–268. doi:10.1016/j.biortech.2012.08.019.

[26] Pham, C. H., Triolo, J. M., & Sommer, S. G. (2014). Predicting methane production in simple and unheated biogas digesters at low temperatures. *Appl. Energy*, *136*, 1–6. doi:10.1016/j.apenergy.2014.08.057.

[27] Rajendran, K., Aslanzadeh, S., & Taherzadeh, M. J. (2012). Household Biogas Digesters—A Review. *Energies*, *5*, 2911–2942. doi:10.3390/en5082911.

[28] Swinbank, W. C. (1963). Long-wave radiation from clear skies. *Q. J. R. Meteorol. Soc.*, *89*, 339–348. doi:10.1002/qj.49708938105.

[29] Terradas-Ill, G., Pham, C. H., Triolo, J. M., Martí-Herrero, J., & Sommer, S. G. (2014). Thermic Model to Predict Biogas Production in Unheated Fixed-Dome Digesters Buried in the Ground. *Environ. Sci. Technol.*, *48*, 3253–3262. doi:10.1021/es403215w.

[30] Wallace, J. M., & Hobbs, P. V. (2006). *Atmospheric Science: An Introductory Survery*. (2nd ed.). Burlington: Academic Press.

[31] Weatherford, V. C. (2010). *Verification of a Thermal Model for Affordable Solar-assisted Biogas Digesters in Cold Climates*. Ph.D. thesis University of Colorado.

[32] Weatherford, V. C., & Zhai, Z. J. (2015). Affordable solar-assisted biogas digesters for cold climates: Experiment, model, verification and analysis. *Appl. Energy*, *146*, 209–216. doi:10.1016/j.apenergy.2015.01.111.

[33] WHO (2016). Household air pollution and health. URL: http://www.who.int/mediacentre/factsheets/fs292/en/.